Multi-scale extensions to quantum cluster methods for strongly correlated electron systems

2009 J. Phys.: Condens. Matter 21 435604

(http://iopscience.iop.org/0953-8984/21/43/435604)

IOP PUBLISHING JOURNAL OF PHYSICS: CONDENSED MATTER

J. Phys.: Condens. Matter **21** (2009) 435604 (13pp) doi:10.1088/0953-8984/21/43/435604

Multi-scale extensions to quantum cluster methods for strongly correlated electron systems

C Slezak[1], M Jarrell[1], Th Maier[2] and J Deisz[3]

[1] Department of Physics, University of Cincinnati, Cincinnati, OH 45221, USA
[2] Oak Ridge National Laboratory, Oak Ridge, TN 37831, USA
[3] Department of Physics, University of Northern Iowa, Cedar Falls, IA 50614, USA

Received 30 May 2009
Published 9 October 2009
Online at stacks.iop.org/JPhysCM/21/435604

Abstract

A numerically implementable multi-scale many-body approach to strongly correlated electron systems is introduced. An extension to quantum cluster methods, it approximates correlations on any given length-scale commensurate with the strength of the correlations on the respective scale. Short length-scales are treated explicitly, long ones are addressed at a dynamical mean-field level and intermediate length-regime correlations are assumed to be weak and are approximated diagrammatically. To illustrate and test this method, we apply it to the one-dimensional Hubbard model. The resulting multi-scale self-energy provides a very good quantitative agreement with substantially more numerically expensive, explicit quantum Monte Carlo calculations.

(Some figures in this article are in colour only in the electronic version)

1. Introduction

Strongly correlated electron systems are characterized by a manifold of complex, competing phenomena, which emerge in the thermodynamic limit. The underlying mechanisms involve correlations on all length-scales. Currently no single feasible numerical method exists to accurately address these correlations at all lengths. Both finite size and mean-field calculations alike are faced with these limitations. However, interest in areas such as quantum phase transitions and magnetically driven superconductivity point to the need for numerical schemes that accurately bridge short and long length-scales.

Quantum cluster techniques [1], constitute a good starting point for addressing the entire range of correlations by dividing the problem into two length regimes; explicitly solving for short ranged correlations and approximately for the remaining longer length-scales. One such method, the dynamical cluster approximation (DCA) [2], maps the lattice problem onto an embedded cluster problem. In so doing, short ranged correlations within a given cluster are treated accurately while the remaining longer ranged correlations are approximated on a dynamical mean-field level. However, the extent of length-scales which can thus be accurately addressed beyond the mean-field level is severely limited by the numerical expense involved.

This limitation results in an inadequate treatment of medium ranged correlations which are outside the scope of explicit calculations. We introduce a multi-scale many-body (MSMB) approach which addresses each length-scale using approximations adequate for the strength of the correlations on the respective scale. The strongest, local and short ranged correlations are well accounted for in traditional, numerically exact implementations of the DCA. Correlations, except for in the vicinity of phase transitions, fall off rapidly with distance and are hence considered weaker in the intermediate length-regime. However, these correlations remain significant and will hence be approximated diagrammatically. Only the remaining third regime of the longest length-scale will be treated at the dynamical mean-field level.

The perturbative inclusion of correlations on an intermediate length-scale within a multi-scale approach has previously been explored by Hague *et al* [3]. Contributions to the single-particle self-energy on various scales were linked in a hybrid approach. However, the inherent perturbative nature of the approach limited it to high temperatures and/or weak coupling strengths. In this work we present a non-perturbative

two-particle diagrammatic approach to the intermediate length-regime.

To illustrate and test this scheme, this MSMB is applied to the one-dimensional Hubbard model [4]. While a formally simple model, the Hubbard model contains much of the underlying physics of correlated electron systems. It is therefore an ideal benchmark for the method. We show that the MSMB approach yields results in very good quantitative agreement with explicit large cluster calculations.

Before we proceed to provide detailed results in section 5 we first establish the theoretical basis for the method. A subsequent outlook on further developments in MSMB techniques is provided in section 6, concluding with a brief summary.

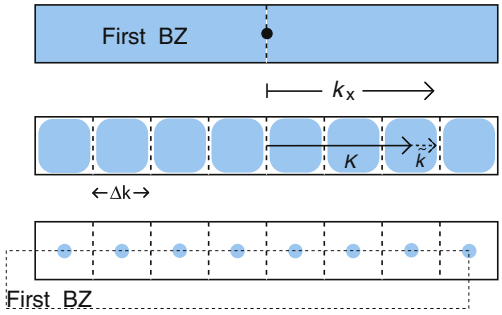

Figure 1. In the DMFA all electron propagators are averaged over the entire BZ, effectively mapping the lattice onto a single point (top). In the DCA, we break the BZ into several sub-cells which are now in turn averaged over mapping the lattice onto a finite sized cluster (bottom).

2. Formalism

For simplicity, we will use the one-dimensional Hubbard model to illustrate the MSMB formalism. This low dimension is also the most difficult regime for quantum cluster approaches like the DCA. The Hubbard Hamiltonian is given by

$$H = -\sum_{\langle ij\rangle} t(c^{\dagger}_{i\sigma}c_{j\sigma} + \text{H.c.}) + \epsilon\sum_{i\sigma} n_{i\sigma} + U\sum_{i}(n_{i\uparrow} - 1/2)(n_{i\downarrow} - 1/2) \quad (1)$$

with $c^{\dagger}_{i\sigma}$ creating an electron of spin σ at site i and local density $n_{i\sigma} = c^{\dagger}_{i\sigma}c_{i\sigma}$. The first part, the kinetic term, allows hopping between adjacent lattice sites with transfer integral t. The second term is the on-site Coulomb repulsion making a doubly occupied lattice site unfavorable. Throughout the remainder of this paper we choose the bare bandwidth $W = 4t$ as the unit of energy by setting $t = 0.25$ and work at fixed filling $n = 0.75$.

2.1. DCA

The DCA is a systematic quantum cluster theory that maps the lattice problem onto a self-consistently embedded cluster problem. It is an extension of the dynamical mean-field theory (DMFT) [5, 6] which systematically incorporates non-local correlations. In the limit when the cluster size is one (i.e. a single site), it recovers the purely local DMFT solution, systematically incorporates non-local corrections as the cluster size increases, and finally becomes exact when the cluster size equals the size of the lattice.

The respective approximations for the DMFT and DCA may be derived by approximating the Laue function which describes momentum conservation at the vertices of the irreducible diagrams:

$$\Delta_{(k_1,k_2,k_3,k_4)} \equiv \sum_{r} \mathrm{e}^{\mathrm{i}r(k_1+k_2-k_3-k_4)} \quad (2)$$

$$\Delta_{\text{exact}} = N\delta_{k_1+k_2,k_3+k_4}. \quad (3)$$

In the DMFT, the Laue function is approximated with $\Delta_{\text{DMFT}} = 1$ for all combinations of k_1, k_2, k_3 and k_4. In doing so, all electron propagators in the self-energy diagrams may be averaged over the first Brillouin zone (BZ), thus relinquishing any momentum dependence of the self-energy. Hence, the DMFT lattice Green's function contains local correlations of the system but is unable to capture non-local correlations. The DCA sets out to systematically include these non-local contributions. This is accomplished by partially restoring momentum conservation of the irreducible vertices. We divide the BZ into N_c identical discrete sub-cells as illustrated in figure 1. The center of each cell is labeled by K, and the surrounding points by $\tilde{k}$, so that any arbitrary $k = K + \tilde{k}$. In the DCA, this partial momentum conservation is expressed by the Laue function:

$$\Delta_{\text{DCA}} = N_c\delta_{K_1+K_2,K_3+K_4}. \quad (4)$$

Therefore, all propagators may freely be summed over intra-cell momenta $\tilde{k}$, yielding the coarse grained Green's function

$$\bar{G}(K, \mathrm{i}\omega_n) = \frac{N_c}{N}\sum_{-\frac{\Delta k}{2}<\tilde{k}\leqslant\frac{\Delta k}{2}} G(K+\tilde{k}, \mathrm{i}\omega_n). \quad (5)$$

In so doing, only momentum conservation of magnitude $\Delta k < (2\pi/N_c)$ is neglected, while larger inter-cell transfers are preserved. The resulting self-energy diagrams are now those of a finite cluster of size N_c where each lattice propagator has been replaced by its coarse grained analog, and the remaining cluster problem is defined by $\bar{G}(K, \mathrm{i}\omega_n)$. We can write for the DCA lattice Green's function

$$G(K+\tilde{k}, \mathrm{i}\omega_n) = \frac{1}{\mathrm{i}\omega_n + \mu - \epsilon(K+\tilde{k}) - \Sigma(M(K+\tilde{k}), \mathrm{i}\omega_n)} \quad (6)$$

where $M(k)$ is a function which maps momentum k residing in a certain sub-cell of the BZ to its cluster momentum K and the lattice self-energy is approximated by that of the cluster problem.

The remaining embedded cluster problem must be solved with a self-consistency requirement that the Green's function calculated on the cluster $G_c(K, \mathrm{i}\omega_n) = \bar{G}(K, \mathrm{i}\omega_n)$. Figure 2 depicts the corresponding DCA algorithm: starting with an initial guess for the self-energy, we construct the coarse grained Green's function $\bar{G}$ from the corresponding lattice G (see equation (5)). In the next step, we utilize one of the many

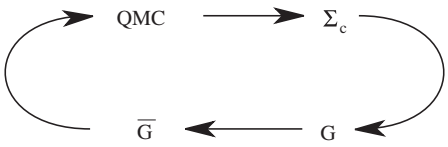

Figure 2. Self-consistency loop for the DCA.

available cluster solvers to determine the cluster self-energy. This is the numerically most involved step and a variety of numerical techniques may be applied. At this point, we use the new estimate for the self-energy to re-initialize the self-consistency loop. It is important to notice that in this procedure only the irreducible lattice quantities are approximated by their cluster equivalent, i.e. the self-energy.

The DCA has been successfully implemented with a variety of cluster solvers, of which some are exact but limited in cluster size while others are applicable up to larger length-scales but involve varying degrees of approximation. Some of the cluster solvers which have been used in conjunction with the DCA include the non-crossing approximation (NCA) [7], the fluctuation exchange approximation (FLEX) [3, 8] and the quantum Monte Carlo (QMC) [2] method. While NCA and FLEX involve various levels of approximations, QMC is of special interest since it provides an essentially numerically exact solution to the problem. Although the QMC constitutes a precise cluster solver, it becomes prohibitively expensive for large clusters. The range of applicability of exact calculations is thus restricted to relatively short length-scales. However, various properties of strongly correlated systems are not accounted for (e.g. the Mermin–Wagner theorem [9]) due to the absence of long ranged fluctuations in these solutions.

2.2. Multi-scale method

The inability of a single solver within the DCA to numerically address long ranged correlations explicitly motivates a MSMB approach where the problem is divided further, incorporating a third, intermediate length-regime. In this approach, the lattice problem is mapped onto two clusters of different size, each of which contributes correlations of length-scales up to the linear extent of their respective cluster size. The respective cluster problems are addressed using approximations adequate with the strength of the correlations on the respective scale. We choose a small DCA cluster of size $N_c^{(1)}$ to be solved using the QMC, thus explicitly accounting for the shortest ranged correlations in the system. Next, we invoke a second, larger cluster of size $N_c^{(2)}$ to address the intermediate length-regime. Except in the vicinity of phase transitions, correlations on these longer length-scales are weaker and the corresponding self-energy is approximated diagrammatically.

We build a suitable approximation by considering the single-particle self-energy (the Hartree term is not explicitly shown) written in terms of the reducible vertex F in both the particle–hole and particle–particle channel as depicted in figure 3. F in turn is related to the irreducible vertex Γ via the Bethe–Salpeter equation (see figure 4).

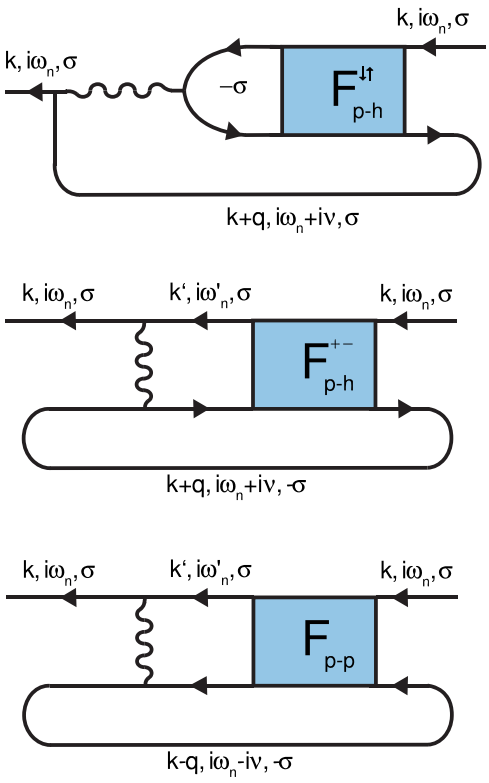

Figure 3. Diagrams relating the self-energy to the reducible two-particle longitudinal spin and charge (top) and transverse spin (middle) vertices. A similar relation is obtained for the particle–particle channel (bottom).

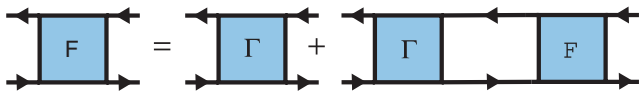

Figure 4. Bethe–Salpeter equation relating the reducible two-particle vertex F to the irreducible vertex function Γ.

$$F(k,k',q;\mathrm{i}\omega_n,\mathrm{i}\omega_n',\mathrm{i}\nu) = \Gamma(k,k',q;\mathrm{i}\omega_n,\mathrm{i}\omega_n',\mathrm{i}\nu) + \Gamma(k,k'',q;\mathrm{i}\omega_n,\mathrm{i}\omega_n'',\mathrm{i}\nu)\chi^0(k'',q;\mathrm{i}\omega_n,\mathrm{i}\nu) \times F(k'',k',q;\mathrm{i}\omega_n'',\mathrm{i}\omega_n',\mathrm{i}\nu). \quad (7)$$

In perturbation theory, the approximations to the self-energy are often made at the level of the irreducible vertex function. In the simple approximation $\Gamma = U$, the resulting self-energy diagrams in figure 3 are those of the FLEX. The resulting method provides qualitatively correct long range properties, but short ranged correlations are addressed inadequately, e.g. local moment formation.

Failure of the FLEX, and similar perturbative approaches based on the irreducible vertex, occurs in the stronger coupling regime. This is a result of neglecting higher order correction terms which renormalize the vertex. In a non-perturbative approach, Vilk *et al* in [10] considered a renormalized static vertex to address this problem.

In the MSMB method, however, we introduce the following non-perturbative approximation for the intermediate length-regime: the large cluster irreducible two-particle vertex is approximated by the small cluster irreducible vertex thus preserving the exact short ranged correlation (on the small

cluster) and approximating the intermediate ranged ones (on the large cluster):

$$\Gamma(K_2, K_2', Q_2; \mathrm{i}\omega_n, \mathrm{i}\omega_n', \mathrm{i}\nu) \rightarrow \Gamma(K_1, K_1', Q_1; \mathrm{i}\omega_n, \mathrm{i}\omega_n', \mathrm{i}\nu) \tag{8}$$

where momenta labeled with subscript 1 are cluster momenta on the small cluster, while the subscript 2 denotes large cluster momenta. The approximated self-energy on the large cluster is evaluated from the Dyson equation depicted in figure 3. It preserves all short ranged correlations and includes long wavelength contributions which emerge from the inclusion of large cluster corrections through the bare bubble χ^0, i.e. the reducible part of the vertex. However, by implementing the DCA on a two-particle irreducible level (i.e. replacing the large cluster irreducible vertex with the small cluster equivalent), the resulting self-energy is inherently different from the single-particle DCA self-energy that one would obtain from the usual, direct DCA/QMC simulation of the large cluster (see section 2.1). Only in the case of infinite dimensions, where the problem becomes purely local, are these two approaches equivalent.

A few remarks about the above approximation are in order. The approximation in equation (8) breaks the crossing symmetry of F (as it is related to Γ by equation (7)), since F now contains long ranged corrections beyond the linear extent of the small cluster only in the channel in which it is calculated. Hence, the self-energy contributions have to be evaluated in all three depicted channels (see figure 3). Furthermore, this MSMB approach requires a full knowledge of the momentum and frequency exchange on the cluster, and hence the evaluation of Γ on the small cluster still involves extensive numerical calculations and is limited by storage/memory requirements (see section 6 for details).

This difficulty of obtaining the small cluster irreducible vertex, Γ, necessitates a further long ranged approximation for Γ. In [14] Abrikosov *et al* have, in their study of Fermi liquid theory, identified a sub-class of self-energy diagrams which convey the long length-scale properties of a system. These are constructed from irreducible vertex functions with zero external momentum and frequency transfer. In applying this restriction we expect to capture long ranged correlations which are characterized by small momentum transfers q. The resulting long wavelength approximated irreducible vertex, denoted by the index λ, is given by

$$\Gamma(K_1, K_1', Q_1; \mathrm{i}\omega_n, \mathrm{i}\omega_n', \mathrm{i}\nu_n) \rightarrow \Gamma^{\lambda}(K_1, K_1', Q_1 = 0; \mathrm{i}\omega_n, \mathrm{i}\omega_n', \mathrm{i}\nu_n = 0). \tag{9}$$

The MSMB approximation at the level of the irreducible vertex is expected to provide the best description for the most dominant two-particle processes. Furthermore, any phase transitions would manifest themselves in instabilities of the reducible vertex which contains the singular structure while the irreducible vertex would remain analytic throughout. However, the MSMB result is expected to remain most valid away from phase transitions where intermediate ranged correlations are weak. When these correlations are not weak, a diagrammatic approximation of the self-energy may contain significant errors, but such an approach can nonetheless represent non-trivial aspects of strong correlations such as non-Fermi liquid behavior [15, 16]. Further details on the calculation of the λ self-energy are provided in section 3.

The self-energy obtained in this λ-approximation only correctly accounts for long ranged fluctuations of the system. The remaining short length-scale contributions have been neglected and have to be accounted for separately, as will be discussed in a subsequent section 2.4.

2.3. A conserving approximation

There are currently two widely used approaches which are sufficient to show that an approximation is conserving. For one, Baym (see [11]) has shown that, with local conservation of spin, charge, momentum and energy at each vertex, it is sufficient for the irreducible vertex to be a functional derivative of the large cluster self-energy $\Gamma(G(K,\omega), U) = \delta\Sigma(G(k,\omega), U)/\delta G(k,\omega)$. However, within both the DMFT and DCA momentum conservation is partially violated at each of the internal vertices as described by their respective Laue functions (equation (2)). This violates certain Ward identities, and hence neither the DMFT nor the DCA constitutes a conserving approximation (see [12] for details).

In an alternative approach, following the arguments of Baym and Kadanoff [13], an approximation can also be shown to be conserving as long as it fulfills both the requirements of (1) the inversion symmetries of F to be preserved and (2) that the two-particle correlation function tends to the single-particle Green's functions via the Dyson equation. It is straightforward to show that the approximation for the self-energy on the large cluster satisfies these requirements. Thus, the MSMB *formalism* based on the explicit small cluster vertex (equation (8) only) constitutes a conserving approximation for the large cluster as it restores momentum dependence of the large cluster self-energy.

With the introduction of the λ-approximation (equation (9)) short ranged correlations are neglected and have to be supplemented as discussed in the subsequent section. The resulting self-energy breaks the conservation laws with corrections of order $1/L_{\mathrm{c}}^{(2)}$ (where $L_{\mathrm{c}}^{(2)}$ is the linear size of the larger cluster). It should be reiterated, however, that the need for the second (long wavelength) approximation is only temporary until the hurdle of large memory requirements can be met.

2.4. Ansatz

To account for the omitted set of short length-scale self-energy diagrams in the λ-approximation, we substitute appropriate diagrams from the small cluster QMC result. This diagrammatic substitution between the different length-scales in the MSMB method is done by means of an analytic ansatz.

One possible implementation of the MSMB method which yields a self-energy containing correlations on both long and short length-scales is given by the real-space ansatz:

$$\Sigma^{(N_{\mathrm{c}}^{(2)})}(x_i, x_j) = \begin{cases} \Sigma_{\mathrm{QMC}}^{(N_{\mathrm{c}}^{(1)})}(x_i - x_j), & |x_i - x_j| \leqslant \frac{N_{\mathrm{c}}^{(1)}}{2} \\ \Sigma_{\lambda}^{(N_{\mathrm{c}}^{(2)})}(x_i - x_j), & \frac{N_{\mathrm{c}}^{(1)}}{2} < |x_i - x_j| \leqslant \frac{N_{\mathrm{c}}^{(2)}}{2} \\ 0, & \text{otherwise.} \end{cases} \tag{10}$$

In this formalism, the MSMB self-energy is constructed by taking all contributions of lengths up to the linear sizes of the small cluster ($N_c^{(1)}/2$) from the exact QMC result and the remaining longer ranged contributions are complemented by the λ-approximated large cluster self-energy. Note, the multi-scale self-energy obtained in equation (10) has lost its spatial continuity. Fourier-transforming the individual length-scale contributions in equation (10) yields

$$\Sigma^{(N_c^{(2)})}(K_2, i\omega_n) = \Sigma_{\mathrm{QMC}}^{(N_c^{(1)})}(x=0, i\omega_n) + \sum_{i=1,\frac{N_c^{(1)}}{2}} 2\cos(iK_2)\Sigma_{\mathrm{QMC}}^{(N_c^{(1)})}(x=i, i\omega_n) + \sum_{j=\frac{N_c^{(1)}}{2}+1,\frac{N_c^{(2)}}{2}} 2\cos(jK_2)\Sigma_{\lambda}^{(N_c^{(2)})}(x=j, i\omega_n) \quad (11)$$

where only diagonal parts of the Fourier transformed self-energy are considered.

Hague *et al* in [3] considered the following, alternative momentum-space ansatz to combine the different length-scales:

$$\Sigma^{(N_c^{(1)})}(K_1, i\omega_n) = \Sigma_{\mathrm{QMC}}^{(N_c^{(1)})}(K_1, i\omega_n) - \Sigma_{\lambda}^{(N_c^{(1)})}(K_1, i\omega_n) + \bar{\Sigma}_{\lambda}^{(N_c^{(2)})}(K_1, i\omega_n) \quad (12)$$

$$\Sigma^{(N_c^{(2)})}(K_2, i\omega_n) = \Sigma_{\lambda}^{(N_c^{(2)})}(K_2, i\omega_n) + \bar{\Sigma}_{\mathrm{QMC}}^{(N_c^{(1)})}(K_2, i\omega_n) - \bar{\Sigma}_{\lambda}^{(N_c^{(1)})}(K_2, i\omega_n) \quad (13)$$

where $\Sigma_{\lambda}^{(N_c^{(1)})}$ is the self-energy obtained in the λ-approximation when implemented on the small cluster. The self-energies $\Sigma^{(N_c^{(1)})}$ and $\Sigma^{(N_c^{(2)})}$ on the small and large cluster, respectively, exist on different grid sizes, and it becomes necessary to convert self-energies from one to the other. This conversion is denoted by a bar over the self-energy which denotes an interpolation when going from a coarser grid to a finer one and a coarse graining step otherwise. For example, the large cluster self-energy $\Sigma^{(N_c^{(2)})}$ is constructed from the explicit λ-approximated self-energy on the large cluster, and two interpolated small cluster (denoted by the superscript $(N_c^{(1)})$) self-energies $\bar{\Sigma}_{\mathrm{QMC}}^{(N_c^{(1)})}$ and $\bar{\Sigma}_{\lambda}^{(N_c^{(1)})}$. It is important to note that the coarse graining in going from large to small cluster self-energies is not an averaging over electron propagators but the term is used in this context to imply an averaging of the self-energy within a cluster-cell.

While the real-space implementation of the ansatz was a straightforward combination of different length-scale elements, the momentum implementation interpretation is more involved. The λ-method provides an estimate for the set of self-energy diagrams which convey the long ranged correlations of the system. However, since in reciprocal space there is not an explicit separation of length-scales, the remaining short length-scale diagrams which are to be supplied by the QMC calculation have to be identified. This can be accomplished by removing the sub-set of λ-approximated self-energy diagrams on the small cluster from the complete set of the QMC calculation, hence avoiding a double counting of the corresponding self-energy contributions.

Within the traditional form of the DCA, all self-energies are inherently causal for each individual cluster. One consequence of causality is that $-\frac{1}{\pi}\,\mathrm{Im}\,\Sigma(k,\omega) > 0$. In this ansatz based implementation of the MSMB method, however, causality is not inherently guaranteed. The combination of self-energy contributions of various length-scales in the ansatz is only ensured to yield a causal multi-scale self-energy in the limit of the cluster sizes approaching one another. Therefore, causality in these schemes cannot be guaranteed and hence has to be monitored closely throughout. For a more detailed discussion of this and the entire momentum-space ansatz see [3].

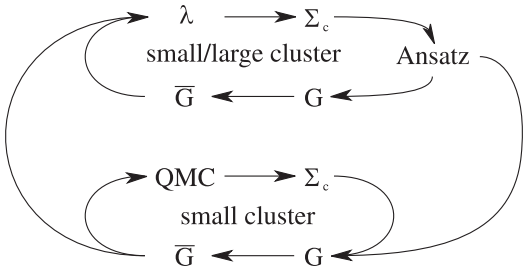

Figure 5. Flow chart for the ansatz self-consistent implementation of the MSMB/DCA.

The remaining self-consistent implementation of the multi-scale method (i.e. two cluster DCA) is similar to that of the traditional, single cluster DCA. Figure 5 depicts a flow chart of the implementation of both ansätze in the scheme of the overall self-consistency loop. The bottom loop shows the already discussed DCA self-consistency loop using the QMC as a small cluster solver. For the large cluster solver (λ-method) the self-consistency is similar. In the overall scheme of the ansatz, the two cluster problems are combined in a fully self-consistent approach: after each iteration of the QMC/DCA loop, the corresponding λ/DCA contribution on the large cluster is evaluated. The ansatz is used after each step to calculate new estimates for the self-energies on both the small and large cluster, thus yielding a fully self-consistent solution. The corresponding paths are shown in figure 5. The converged ansatz self-energy will be dominated by the small cluster QMC self-energy which contributes the strongest, short ranged correlations. The remaining weaker long ranged correlations are incorporated in the difference of λ-approximated self-energies between the two clusters. In moving away from a fully self-consistent approach, the self-consistency restrictions may be lessened to various degrees. Some possible implementations will be discussed in further detail in section 4.

3. Approximations to the vertex

In this section we provide the remaining details of the λ-approximation. Previous studies, as well as our own results, have shown that in the positive U Hubbard model the long ranged contributions to the self-energy are dominated by the spin and charge fluctuations of the system. In contrast, pairing fluctuations are less significant and do not change the qualitative multi-scale results, unless very low temperatures

are considered. The self-energy determination in the results section for the lowest order in U approximation to Γ^λ considers all three channels. However, the remaining higher order cases are restricted to only the self-energy contribution of the particle–hole channel. An equivalent derivation to the following can be trivially extended to the particle–particle channel.

Starting with the λ-approximation introduced in section 2.2 (equations (8) and (9)), the Bethe–Salpeter equation (equation (7)) for the approximated large cluster reducible vertex function can be coarse grained to the small cluster (see section 6 for further details):

$$\begin{aligned}\bar{F}^\lambda(K_1, K_1', Q_2; \mathrm{i}\omega_n, \mathrm{i}\omega_n', \mathrm{i}\nu) &= \Gamma^\lambda(K_1, K_1'; \mathrm{i}\omega_n, \mathrm{i}\omega_n') \\ &+ \Gamma^\lambda(K_1, K_1''; \mathrm{i}\omega_n, \mathrm{i}\omega_n'')\bar{\chi}^0(K_1'', Q_2; \mathrm{i}\omega_n, \mathrm{i}\nu) \\ &\times \bar{F}^\lambda(K_1'', K_1', Q_2; \mathrm{i}\omega_n'', \mathrm{i}\omega_n', \mathrm{i}\nu) \end{aligned} \tag{14}$$

where we coarse grained the bare particle–hole susceptibility bubble (internal legs in figure 4 which are lattice Green's functions). We call this coarse grained susceptibility $\bar{\chi}^0$

$$\begin{aligned}\bar{\chi}^0(K_1'', Q_2; \mathrm{i}\omega_n, \mathrm{i}\nu) &= -\frac{TN_\mathrm{c}}{N}\sum_{\tilde{k}'', \mathrm{i}\omega_n} G(K_1'' + \tilde{k}'', \mathrm{i}\omega_n'') \\ &\times G(K_1'' + \tilde{k}'' + Q_2, \mathrm{i}\omega_n'' + \mathrm{i}\nu). \end{aligned} \tag{15}$$

Furthermore, while the coarse graining (sum over internal moment $\tilde{k}''$) is to the small cluster, the self-energy in G originates from the large cluster. The resulting reducible vertex function $\bar{F}^\lambda$, however, is still only defined for small cluster momenta but incorporates large cluster corrections from the coarse grained susceptibility $\bar{\chi}^0$. Due to these long ranged contributions, the reducible vertex constructed in this manner is not equivalent to a QMC evaluated small cluster F.

The resulting Bethe–Salpeter equation (14) is most easily solved for $\bar{F}^\lambda$ in the following matrix form:

$$\bar{F}^{(\lambda)-1}(Q_2, \mathrm{i}\nu) = \Gamma^{(\lambda)-1} - \bar{\chi}^0(Q_2, \mathrm{i}\nu) \tag{16}$$

where the matrix indices correspond to the internal momenta and frequency.

At this point, the self-energies can now finally be evaluated using the Dyson equation as illustrated in figure 3. On the large cluster this yields

$$\begin{aligned}\Sigma_\lambda^{(N_\mathrm{c}^{(2)})}(K_2, \mathrm{i}\omega_n) &= \frac{UT^2}{N_\mathrm{c}^{(1)}N_\mathrm{c}^{(2)}}\sum_{K_1', Q_2, \mathrm{i}\omega_n', \mathrm{i}\nu} G(K_2 + Q_2, \mathrm{i}\omega_n + \mathrm{i}\nu) \\ &\times \bar{\chi}^0(K_1', Q_2; \mathrm{i}\omega_n', \mathrm{i}\nu) \\ &\times (\bar{F}^{\lambda+-}(K_1', M(K_2), Q_2; \mathrm{i}\omega_n', \mathrm{i}\omega_n, \mathrm{i}\nu) \\ &- \bar{F}^{\lambda\uparrow\downarrow}(K_1', M(K_2), Q_2; \mathrm{i}\omega_n', \mathrm{i}\omega_n, \mathrm{i}\nu) - U). \end{aligned} \tag{17}$$

Here we interpolate the small cluster momentum $M(K_2) \to K_2$ (for details see section 6) and subtract U in the parenthesis to prevent over counting of the second order term.

In the calculation of the transverse spin fluctuation part recall that $2\chi^\pm = \chi^{zz}$, where we define $\chi^\pm$ as the correlation function of σ^+ and σ^-, and χ^{zz} as the correlation function formed from σ^z. Then as $\chi^{zz} = 2(\chi^{\uparrow\uparrow} - \chi^{\downarrow\uparrow})$, we have that $\chi^\pm = \chi^{\uparrow\uparrow} - \chi^{\downarrow\uparrow}$ and $F^\pm = F^{\uparrow\uparrow} - F^{\downarrow\uparrow}$. This means that for the self-energy on the large cluster

$$\begin{aligned}\Sigma_\lambda^{(N_\mathrm{c}^{(2)})}(K_2, \mathrm{i}\omega_n) &= -\frac{UT^2}{N_\mathrm{c}^{(1)}N_\mathrm{c}^{(2)}}\sum_{K_1', Q_2, \mathrm{i}\omega_n', \mathrm{i}\nu} G(K_2 + Q_2, \mathrm{i}\omega_n + \mathrm{i}\nu) \\ &\times (2\bar{F}^{\lambda\uparrow\downarrow}(K_1', M(K_2), Q_2; \mathrm{i}\omega_n', \mathrm{i}\omega_n, \mathrm{i}\nu) + U) \\ &\times \bar{\chi}^0(K_1', Q_2; \mathrm{i}\omega_n', \mathrm{i}\nu). \end{aligned} \tag{18}$$

While for the real-space implementation of the ansatz, knowledge of the large cluster self-energy in the λ-approximation is sufficient, the momentum-space version requires the corresponding self-energy diagrams on the small cluster as well. An equivalent calculation on the small cluster yields for the self-energy in the λ-approximation

$$\begin{aligned}\Sigma_\lambda^{(N_\mathrm{c}^{(1)})}(K_1, \mathrm{i}\omega_n) &= -\frac{UT^2}{N_\mathrm{c}^{(1)^2}}\sum_{K_1', Q_1, \mathrm{i}\omega_n', \mathrm{i}\nu} G_\mathrm{c}(K_1 + Q_1, \mathrm{i}\omega_n + \mathrm{i}\nu) \\ &\times (2F_\mathrm{c}^{\lambda\uparrow\downarrow}(K_1', K_1, Q_1; \mathrm{i}\omega_n', \mathrm{i}\omega_n, \mathrm{i}\nu) + U) \\ &\times \chi_\mathrm{c}^0(K_1', Q_1; \mathrm{i}\omega_n', \mathrm{i}\nu) \end{aligned} \tag{19}$$

where all single-particle propagators have been replaced by G_c, including the ones entering the bare bubble χ^0.

We want to reiterate that the λ-approximated self-energy thus obtained is only accurate for long ranged correlations. In order to obtain a viable multi-scale solution, the neglected short ranged correlations have to be accounted for by means of the ansatz, as outlined in section 2.

3.1. First order in U

The introduced non-perturbative MSMB method requires a detailed knowledge of the small (QMC) cluster irreducible vertex. This evaluation of Γ, however, poses a difficult and numerically involved problem. We shall therefore initially only consider perturbative approximations to the vertex within the MSMB method. In approximating the irreducible vertex by the frequency independent first order contribution, i.e. $\Gamma(K, K'; \mathrm{i}\omega_n, \mathrm{i}\omega_n') = U$, the self-energy diagrams of figure 3 reduce to the well known FLEX [17–19] diagrams. In the particle–hole channel, the corresponding self-energy is given by

$$\Sigma^{(\mathrm{ph})}(k, \omega_n) = \frac{UT}{N}\sum_q\sum_m V^{(\mathrm{ph})}(q, \omega_m)G(k - q, \omega_n - \omega_m). \tag{20}$$

The FLEX potential is defined by

$$\begin{aligned}V^{(\mathrm{ph})} &= \chi_\mathrm{ph}^0(q, \omega_n) - \frac{1}{2}\frac{\chi_\mathrm{ph}^{0\,2}(q, \omega_n)}{1 + \chi_\mathrm{ph}^0(q, \omega_n)} \\ &+ \frac{3}{2}\frac{\chi_\mathrm{ph}^{0\,2}(q, \omega_n)}{1 - \chi_\mathrm{ph}^0(q, \omega_n)} \end{aligned} \tag{21}$$

where

$$\chi_\mathrm{ph}^0(q, \omega_n) = -\frac{T}{N}\sum_k\sum_\omega G(k, \omega_m)G(k+q, \omega_m+\omega_n). \tag{22}$$

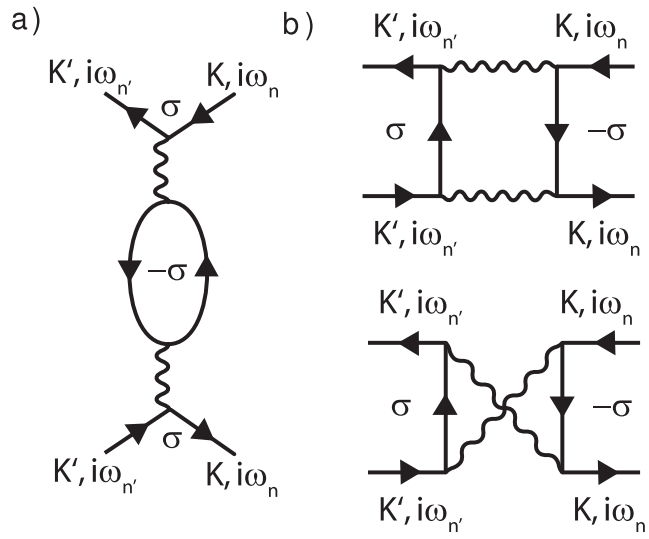

Figure 6. Second order diagrams for the vertex functions $\Gamma^2_{\uparrow\uparrow}$ (a) and $\Gamma^2_{\uparrow\downarrow}$ (b) for an external momentum transfer $q = 0$.

Using the FLEX to address the long length-scale problem within a multi-scale method was the scope of the work by Hague [3]. Initially we will return to this simple cluster solver which is known to provide qualitatively correct long length-scale properties. We will use the FLEX to illustrate some of the properties and problems associated with the ansatz in momentum-space (see equations (12) and (13)). After exploring some of the limitations encountered, we will introduce variations of the original implementation which expand the scope of applicability of the FLEX within the MSMB scheme.

3.2. Second order in U

At lower temperature, or for larger U, higher order terms in the vertex are important. The second order corrections to the irreducible vertex function in the λ-approximation (i.e. zero external momentum transfer $q = 0$ and frequency $\nu_n = 0$) are shown in figure 6. The irreducible vertex is given in the spin channel by

$$\Gamma^{(\lambda)s}(i\omega_n, i\omega_{n'}; K_1, K_1') = -U - \frac{U^2 T}{N_c^{(1)}} \sum_{i\omega_{n''}, K_1''} G(i\omega_{n''}, K_1'') \times G(i\omega_n + i\omega_{n'} - i\omega_{n''}, K_1 + K_1' - K_1'') \quad (23)$$

and in the charge channel

$$\Gamma^{(\lambda)c}(i\omega_n, i\omega_{n'}; K_1, K_1') = +U + \frac{U^2 T}{N_c^{(1)}} \sum_{i\omega_{n''}, K_1''} G(i\omega_{n''}, K_1'') \times (G(i\omega_n + i\omega_{n'} - i\omega_{n''}, K_1 + K_1' - K_1'') + 2G(i\omega_n - i\omega_{n'} + i\omega_{n''}, K_1 - K_1' + K_1'')). \quad (24)$$

3.3. Full QMC vertex

In the non-perturbative MSMB approach the full irreducible vertex, as obtained by the QMC, is considered. Within the QMC algorithm we are unable to determine Γ directly and instead calculate the two-particle correlation function χ. The irreducible vertex function can be found by inverting the Bethe–Salpeter equation. In the spin channel we have the two-particle correlation function

$$\chi^s = \chi^0 + \chi^0 \Gamma^s \chi^s \quad (25)$$

which is a matrix with elements both in frequency and momentum (the same holds for the charge channel). The irreducible spin vertex is denoted by Γ^s and χ^0 is the bare spin susceptibility. The correlation functions are evaluated in the QMC by sampling over the configuration space (Hirsch–Hubbard–Stratonovich fields [2]) in one of two ways, each one posing its own challenges.

One possibility is directly evaluating $\chi(i\omega_n, k; i\omega_{n'}, k')$ in frequency space. This requires the individual QMC Green's function to be Fourier transformed (FT) from the time domain. However, since the calculation is limited to finite time intervals $\Delta\tau$ the FT will incur substantial high-frequency artifacts. In theory this can be improved by means of a high-frequency conditioning, but no analytic form is available within the QMC calculation to facilitate such a conditioning. The resulting substantial artifacts are propagated into the irreducible vertex function.

Alternatively χ can be evaluated in the time domain and only Fourier transformed once the QMC averaging is complete. This results in an accurate measurement of the two-particle correlation function by the QMC but is significantly more computationally expensive. Although this approach provides an accurate measure for $\chi(\tau_1, \tau_2; \tau_3, \tau_4)$, the Bethe–Salpeter equation cannot be used to solve for Γ in the time domain and hence the QMC averaged χ has to be Fourier transformed first. This once again results in similar problems associated with the FT. In the high temperature regime where higher order corrections in U are not important a perturbative approach to high-frequency conditioning of the FT is very successful. However, as the temperature is lowered and the significance of higher order corrections within the vertex grows, this conditioning results in even larger artifacts. Therefore we use the frequency domain in our determination of χ.

4. Technical aspects

A MSMB approach based on a first order approximated vertex is similar to the limited FLEX-hybrid approach previously considered by Hague *et al* [3]. In their work the intermediate length-regime was addressed using FLEX which was incorporated within a multi-scale approach using the fully self-consistent momentum-space ansatz (see equations (12) and (13)). However, in the regime of stronger couplings and/or lower temperatures, where a significant contribution of longer ranged correlations is to be expected, the method fails. In this section we propose changes to the implementation of the multi-scale method which significantly improves its range of applicability by (1) restriction of the ansatz to the large cluster, (2) modification of the cluster conversion, and (3) removal of the self-consist implementation of the ansatz on the large cluster.

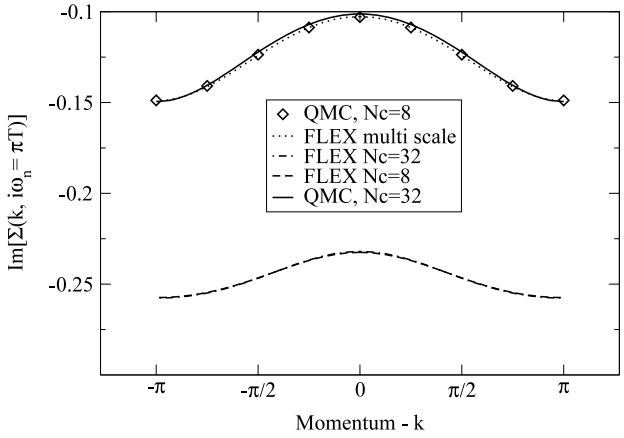

Figure 7. Imaginary part of the self-energy at the lowest Matsubara frequency as obtained by various cluster solvers and the FLEX/MSMB method at $\beta = 8$, $U = W = 1.0$, and $n = 0.75$. The MSMB cluster sizes are $N_c^{(1)} = 8$ and $N_c^{(2)} = 32$.

In the original inception [3], the ansatz is evaluated fully self-consistently within both the QMC and the FLEX as discussed in section 2.4. The self-energy contributions of these two clusters solvers are linked by the momentum-space ansatz. However, long ranged correlations, as are described by the large cluster FLEX, are assumed weak. Hence, their presence in the effective medium of the small cluster only minutely effects the QMC self-energy. We thus neglect the ansatz on the small cluster (equation (12)). With this modification, the small cluster problem can be solved independently of the large cluster problem. This results in a significant reduction in numerical complexity.

With the removal of the small cluster ansatz condition, only a unidirectional cluster conversion of small cluster self-energies to the large cluster remains. In this work, a periodic cubic spline interpolation[4] is employed. This provides a good approximation for the multi-scale self-energy in the high temperature/small U limit. Figure 7 shows the imaginary part of the exact, QMC calculated and FLEX self-energies on both clusters calculated at high T. In this regime, correlations are short ranged in nature and thus well described by the small cluster itself, while the remaining long ranged features, which are provided by the large cluster FLEX, are insignificant. The interpolated small cluster self-energy accurately replicates that of the explicit large single cluster QMC result. This results in a vanishing FLEX contribution within the ansatz as the large and interpolated small cluster FLEX results are identical and thus cancel each other out (see the superimposed, lower set of curves in figure 7).

In this high temperature regime (e.g. figure 7) the fully self-consistent ansatz as well as our modified one remain numerically stable. However, one inherent limitation of the approach is already apparent. The observed magnitude of the negative imaginary part of the QMC self-energy is significantly

[4] We omit the additional coarse graining of the self-energy in the original work. This is deemed appropriate since the interpolated small cluster self-energy won't recoup the lattice self-energy and hence a coarse graining to a cluster is meritless.

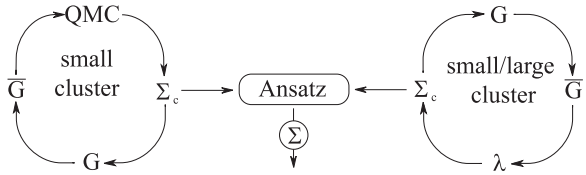

Figure 8. Flow chart depicting two independent self-consistent DCA calculations combined via an ansatz to construct a MSMB self-energy.

smaller than the FLEX result. This overestimation of the self-energy by the FLEX deems a first order approximation to the vertex to be insufficient. A self-consistent implementation of the ansatz aggregates the problem, as the ansatz self-energy used to initialize each FLEX iteration is similar in magnitude to the QMC self-energy. This results in an insufficient damping of the FLEX potentials and the subsequent overestimation of the FLEX self-energy renders the large cluster self-energy calculation numerically unstable. This is an inherent problem in the self-consistent approach. In an attempt to enhance the numerical stability of the MSMB method we remove the self-consistent implementation of the ansatz on the large cluster. This leaves two independent DCA calculations for the small and large cluster which, after the individual problems are converged, are combined by the ansatz. The resulting self-consistency scheme is depicted in figure 8. However, the effective media embedding the two cluster problems now are unaware of correlations determined by the other cluster solver technique. Therefore, the effective medium of the large cluster now lacks the explicit short ranged correlations provided by the QMC. Similarly, the effective medium of the small cluster only contains long ranged correlations provided by the dynamical mean-field approximation.

The third modification enters in the determination of the small cluster FLEX self-energy $\Sigma_{\mathrm{FLEX}}^{(N_c^{(1)})}$. Rather than calculating it explicitly, we obtain it by coarse graining the large cluster self-energy onto the small cluster. The combination of all changes introduced up to this point significantly increases the range of low temperatures which can be addressed by a perturbative MSMB approach.

Throughout the remainder of the paper we will restrict ourselves to the non-self-consistent momentum-space ansatz as outlined in this section. It indeed succeeds in addressing some of the problems encountered in the original implementation and yields a numerically stable MSMB method.

5. Results

Throughout the remainder of the paper, we evaluate the quality of the MSMB method by comparing the self-energy to that of a 32-site, single cluster DCA/QMC calculation.

5.1. First order in U

We begin the evaluation of the MSMB method by considering the first order approximation to the irreducible vertex. The previous section introduced a numerically stable approach

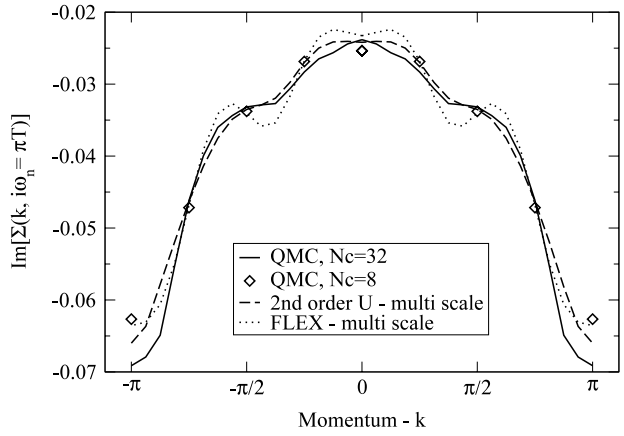

Figure 9. Imaginary part of the self-energy at the lowest Matsubara frequency as obtained by the MSMB method using first order (FLEX) and second order approximated irreducible vertices Γ in comparison to the large single cluster QMC results at $\beta = 31$, $U = W = 1.0$, and $n = 0.75$. Multi-scale results are for cluster sizes $N_c^{(1)} = 8$ and $N_c^{(2)} = 32$.

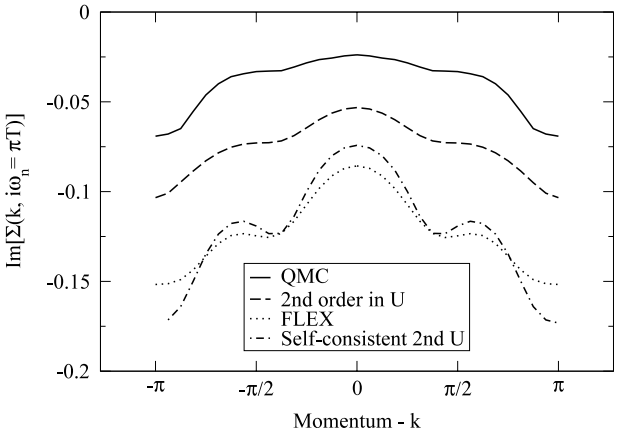

Figure 10. Imaginary part of the λ-approximated self-energy at the lowest Matsubara frequency for the large cluster ($N_c^{(2)} = 32$) using various cluster solvers in comparison to the single cluster QMC result at $\beta = 31$, $U = W = 1.0$, and $n = 0.75$. Also shown is the overestimated ansatz self-consistent self-energy of the MSMB method for the second order approximated Γ.

to the perturbative MSMB method. This allows for the FLEX based MSMB treatment of stronger coupling/lower temperature regimes.

The major limitation of this method, however, remains in the still significant difference in magnitude of the QMC and FLEX self-energies leading to an overestimation of long length-scale features introduced by FLEX. In figure 9 it is quite apparent that at lower temperatures the FLEX MSMB implementation overestimates the size of the long length-scale features, i.e. the amplitude of the oscillations in the imaginary part of the self-energy. This is yet further indication that a bare approximation to the vertex is inadequate to address the intermediate length-regime.

5.2. Second order in U

We move to include second order corrections in the vertex, which is expected to mitigate the effects of the underestimation to the vertex in the FLEX. This lessens the difference in magnitude between the QMC and λ self-energy within the ansatz (as observed in figure 7) and thus increases the applicability of the MSMB method to lower temperatures.

Figure 9 compares the imaginary part of the self-energy at the lowest Matsubara frequency for various degrees of approximation. In contrast to the gross overestimation of the first order approximation to Γ, the inclusion of second order in U corrections within the MSMB method successfully captures the long length-scale features of the large single cluster QMC self-energy throughout most of the BZ. The largest deviations in the multi-scale self-energy are found about the corners of the BZ, i.e. $k = \pm\pi$. Within the ansatz, the difference between the small and large cluster λ self-energies provides the long length-scale features, thus partially restoring the self-energy information which was lost by coarse graining to the small QMC cluster. However, using a λ self-energy with a negative imaginary part which is considerably larger than that of the small cluster QMC results in an overestimation of this correction, predominately in regions encompassed by steep gradients in the self-energy.

Figure 10 further illustrates the pathology of the ansatz associated with the difference in magnitude of the cluster self-energies. We show the imaginary part of the self-energy as obtained by the various λ-approximations on the large cluster in comparison to the large single cluster QMC result. The magnitude of the negative imaginary part of the self-consistent FLEX (first order in U approximation) self-energy is, as was previously indicated, very large compared to the magnitude of the QMC result. The new approach of including second order corrections in U in the vertex function, succeeds in yielding a self-energy which resembles that of the QMC more closely. Similarly to the numeric instability encountered with the FLEX approximation, the self-consistent determination of the λ self-energy using the large cluster ansatz also yields a larger self-energy but does not encounter the catastrophic divergence of the FLEX. We find that a second order Γ combined with a non-self-consistent ansatz provides the best multi-scale solution to the problem.

Now that we have established the viability of the MSMB technique we take a closer look at the dependence of the small cluster size on the quality of the multi-scale result. Within the MSMB method the QMC constitutes the computationally most expensive part. Hence, we want to restrict the calculations to the smallest possible QMC cluster ($N_c^{(1)}$) without any significant loss of quality in the multi-scale results. It is therefore important to study the dependence of the multi-scale results on the size of the small cluster.

Figure 11 shows the multi-scale self-energy for a variety of small cluster sizes as obtained by the MSMB method using the second order approximation to the λ vertex. It is apparent that a cluster size of $N_c^{(1)} = 4$ is too small to adequately capture the main k dependence (overall magnitude) of the QMC's self-energy. Considering such a small QMC cluster grossly misrepresents the range of the QMC self-energy and is not recovered in the MSMB method. This is an indication that

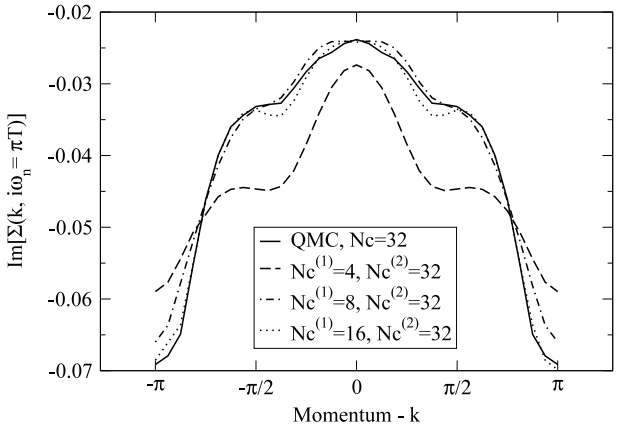

Figure 11. Imaginary part of the self-energy at the lowest Matsubara frequency as obtained by the MSMB approach using the second order λ-approximation and large single cluster QMC. Results are for various small cluster sizes $N_c^{(1)}$ at $\beta = 31$, $U = W = 1.0$, and $n = 0.75$.

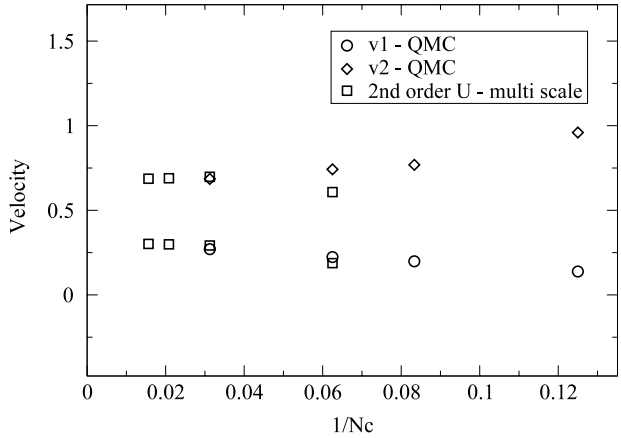

Figure 12. Spin and charge velocities ($v1$ and $v2$, respectively) obtained by fitting the different results with the Luttinger Green's functions (equation (26)) about cluster momentum $k = \pi/2$ for $\beta = 31$, $U = W = 1.0$ and $n = 0.75$. Multi-scale results are for a small cluster size $N_c^{(1)} = 8$ and different large cluster sizes, and the QMC velocities were obtained from a single 32-site cluster calculation.

correlations beyond the length-scales of the small cluster are still significant and not sufficiently well approximated by the λ-method. A small cluster size of $N_c^{(1)} = 8$, on the other hand, appears adequate and only slightly underestimates the self-energy in the vicinity of $k = \pm\pi$. In this area we continually observe significant remnants of the coarse graining of the QMC which is inadequately restored by the MSMB method.

Up to this point we have focused our investigation on the momentum dependence of the self-energy at small Matsubara frequency. Since the visual representation of the self-energy features at multiple, larger Matsubara frequencies would be cumbersome, we proceed to further illustrate the strengths of this MSMB technique by focusing on the presence of spin–charge separation in the system which is manifest in the full frequency dependent self-energy.

One-dimensional systems have been shown to be non-Fermi liquids. Amongst other unique features, they are known to exhibit spin–charge separation [20–22]. This very intriguing property manifests itself by the complete decoupling of spin and charge degrees of freedom. The single-particle spectra of such systems exhibit two unique peaks corresponding to either spin or charge excitations which move independently of each other. Due to the involved nature of extracting spectra from the MSMB method, we are at this time unable to directly identify the presence of any such feature in our results. One characteristic of such a separation, however, is the presence of two distinct velocities corresponding to charge and spin, respectively. Following an approach by Zacher [23], we examine the MSMB Matsubara frequency Green's function for the possible presence of spin–charge separation. This is done by fitting the Green's function obtained from the MSMB method to that of the Luttinger model solution

$$G^{(\mathrm{LM})}_{v_1,v_2,\kappa_\rho}(x,\tau) = \frac{\mathrm{e}^{\mathrm{i}k_F x}c}{\sqrt{v_1\tau + \mathrm{i}x}\sqrt{v_2\tau + \mathrm{i}x}(x^2 + v_2^2\tau^2)^{-(\kappa_\rho+1/\kappa_\rho-2)/8}}, \quad (26)$$

where v_1 and v_2 are the spin and charge velocities and c is a normalization constant. We use the approximation for the correlation exponent $\kappa_\rho = 1$ which is deemed sufficient by Zacher for the purposes of identifying the presence of two different velocities. In order to accurately perform a fit with our data we need to additionally coarse grain (see equation (5)) the Luttinger liquid Green's function to obtain a fitting function in line with the idea of the DCA. This fit yields values for both the spin and charge velocities when fitted at $k = \pi/2$, which is the DCA momentum closest to the Fermi wavevector. This specific choice of k value is motivated by the fact that the Luttinger model solution is based on a low energy approximation of the Hubbard model where a linearized dispersion around the Fermi vector is assumed. For the parameters in figure 12 the Fermi wavevector ($k_F \approx 1.2$) falls into the cluster-cell about $k = \pi/2$.

Figure 12 shows the spin and charge velocities (v_1 and v_2, respectively) obtained by using the single cluster QMC results for smaller cluster sizes and multi-scale results for larger ones. For intermediate cluster sizes, where both the QMC and the MSMB method are feasible, we see a good match between the two methods. For larger cluster sizes where the QMC approach becomes unfeasible the multi-scale results fall close to the QMC extrapolated values. Furthermore, as we extrapolate the multi-scale results to the infinite cluster size limit we find two different velocities: $v_1 = 0.311$ and $v_2 = 0.674$. These values compare rather well to those obtained by Zacher *et al*'s [23] grand-canonical QMC calculation for a cluster size of 64, $\beta = 80$ and all other parameters equal to ours: $v_1 = 0.293 \pm 0.019$ and $v_2 = 0.513 \pm 0.023$. Although the temperature in figure 12 is slightly higher than that of Zacher's results, we observed only a small temperature dependence of the fitted velocities in our calculations. The similarity between the two results are quite remarkable considering that our calculations were based on a substantially smaller eight-site QMC cluster and hence less subject to the sign problem[5]. These are yet

[5] The DCA inherently has a lesser sign problem within the QMC compared to finite size approaches [2] and in the combination with a smaller cluster size results in a significantly larger average sign.

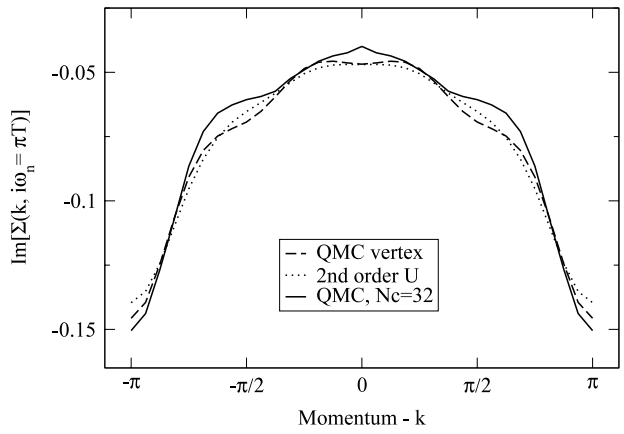

Figure 13. Imaginary part of the self-energy at the lowest Matsubara frequency as obtained by the MSMB method using second order approximated and full QMC evaluated Γs in comparison to large single cluster QMC results at $\beta = 31$, $U = \frac{3}{2}W = 1.5$ and $n = 0.75$. Multi-scale results are for cluster sizes $N_c^{(1)} = 8$ and $N_c^{(2)} = 32$.

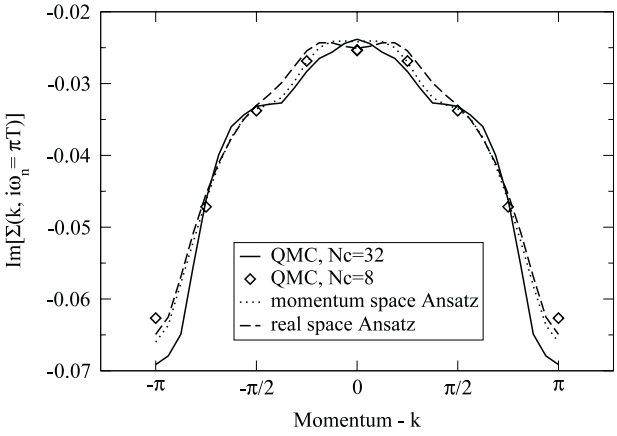

Figure 14. Imaginary part of the self-energy at the lowest Matsubara frequency as obtained by the MSMB method using the second order approximated Γ in conjunction with the real-space and momentum-space based ansatz at $\beta = 31$, $U = W = 1.0$ and $n = 0.75$. Also shown is the large single cluster QMC result. Multi-scale results are for cluster sizes $N_c^{(1)} = 8$ and $N_c^{(2)} = 32$.

further indications that the MSMB method indeed successfully captures the long length-scale physics of the model and is in good quantitative agreement with large single cluster QMC calculations.

5.3. Full QMC vertex

The previous two sections initially considered a first order approximated irreducible vertex function (i.e. the FLEX) and then proceeded to show the significant improvement that can be achieved by including second order corrections to Γ within the MSMB method. Both of these perturbative approaches, however, resulted in an overestimation of the long length-scale features of the self-energy at low temperatures. We now return to the non-perturbative λ-approximation using the irreducible QMC vertex. This approximation is expected to significantly improve the results, especially at lower temperatures where higher order corrections to the bare vertex are important and measurably contribute to the self-energy.

Figure 13 compares the imaginary part of the multi-scale self-energies, obtained by considering both the second order vertex and the full QMC vertex, to the numerically exact large single cluster QMC self-energy. While the resulting multi-scale self-energy utilizing the full vertex function gives a better approximation for some momenta, the second order vertex solution remains preferable for others. This behavior may be somewhat unexpected since the inclusion of higher order corrections in the vertex was expected to further improve the overall quality of the multi-scale solution. However, we believe that this discrepancy arises from difficulties in extracting the exact vertex related to problems with high-frequency conditioning in the QMC and is not an intrinsic problem of the method. As a consequence, the consideration of second order corrections in the λ-approximation remains the most useful at this time. It successfully allows for the exploration of lower temperatures—a regime where the reducible vertex function develops a richness in features.

5.4. Real-space ansatz

Up to this point, the various approximations to the irreducible vertex function within the MSMB technique were implemented using the momentum-space ansatz. We now return to the previously introduced implementation of the real-space ansatz (see equation (11)). The significant difference is that the separation of length-scales in the real-space approach is straightforward, and therefore over counting of diagrams is not an issue. The second order vertex approach was shown to be widely successful and will hence be used to investigate this ansatz implementation as well. It should be noted that both versions of the ansatz are treated identically as far as the implementation of self-consistency is concerned (see section 5.1).

Figure 14 compares the multi-scale self-energy of the two ansatz implementations to the large single cluster QMC result. It is quite apparent that the real-space implementation of the MSMB method is inferior. The momentum-space ansatz provides a self-energy more closely resembling the exact result throughout the BZ.

The real-space ansatz provides an intuitive and simple way to combine the different length-scales of the problem in contrast to a more complicated implementation in momentum-space. Although inferior, the real-space ansatz remains a viable, numerically stable alternative. It furthermore provides an alternative means of interpolating the small cluster self-energy by neglecting the large cluster self-energy contributions in equation (11), which were found to be negligible in this approach. The resulting interpolated small cluster QMC self-energy (not shown) closely resembles that of the real-space ansatz based MSMB method.

6. Numerical considerations and outlook

In the development of this MSMB method we were forced to employ various approximations due to current computational

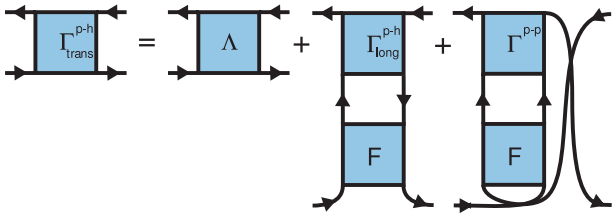

Figure 15. The Parquet equation relating the transverse particle–hole irreducible vertex Γ^{p-h}_{trans} to the fully irreducible vertex Λ plus contributions from the longitudinal and particle–particle cross channels. Similar relations apply for the remaining channels (not shown).

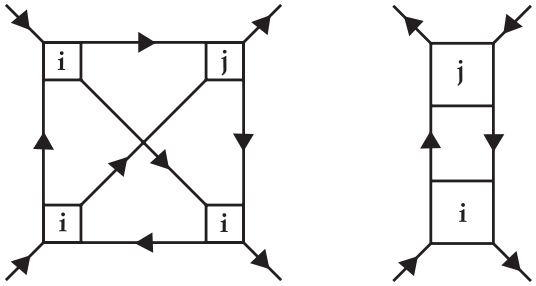

Figure 16. Lowest order non-local corrections to the fully irreducible vertex Λ (left) and the vertex Γ (right).

limitations. The largest numerical concession was made in section 3, where we restricted the calculations of F^{λ} to the small cluster (see equation (14)). Ideally, the irreducible vertices Γ would be interpolated and the full reducible vertex evaluated on the large cluster in turn. This calculation, however, would scale as $(N_c^{(2)} N_l)^4$ (N_l is the number of time-slices in the QMC [2]) and hence provide little advantage over a single cluster QMC calculation. We therefore restrict the evaluation of $\bar{F}^{\lambda}\bar{\chi}^0$ in equation (18) to the small cluster and interpolate the product of χ^0 and F^{λ} to the large cluster.

With the onset of peta-scale computing we will be able to make two fundamental improvements to the MSMB approach in the near future. Initially, we will gain the ability to include the fully momentum and frequency dependent Γ in our calculation, thus eliminating the necessity of the λ-approximation (equation (9)). Inherent in this modification is an explicit account of the correct short ranged physics hence removing the need for the ansatz. However, the memory and CPU requirements for this type of calculation scale as $(N_c^{(1)} N_l)^3$. For a large cluster with $N_c = 16$ and $N_l = 100$, this would require 66 GB of double precision complex storage, far exceeding the memory associated with a single CPU. These staggering memory requirements can currently only be met by some shared-memory parallel processing (SMP) supercomputers.

In the second improvement, the approximation of the large cluster Γ by the small cluster QMC can be replaced by one utilizing the fully irreducible vertex Λ (the vertex which is two-particle irreducible in both the horizontal and vertical plane). This results in a self-consistent renormalization of Γ via the Parquet equations [17, 24], and hence an inclusion of long ranged correlations in the crossing channel (see figure 15) which are missing in both the λ-approximation and the Γ-based approximation described above.

The superiority of the latter approach becomes clear in the high-dimensional limit, where it is Λ, not Γ, which becomes local. This can be shown by considering the simplest non-local corrections to the respective vertices Λ and Γ in figure 16. The boxes represent a set of graphs restricted to site i (local) and j (neighboring), respectively. In the limit of high dimensions, each site i has $2D$ adjacent sites j. The contributions of each leg within the vertex in the limit $D \to \infty$ is $G(r) \sim D^{-r/2}$ (for details see [8]). This results in a contribution to the correction of $\mathcal{O}(D^{-1})$ for the two legs in Γ and $\mathcal{O}(D^{-3/2})$ for Λ. Thus, the non-local corrections to Λ including all neighboring sites j falls off as $D^{-1/2}$ and becomes local in the infinite-dimensional limit. In contrast, the corrections to Γ remain of order one. Therefore, in the high-dimensional limit, Λ is local while Γ has non-local corrections. In finite dimensions, we would expect that Λ is more compact than Γ whenever the single-particle Green function falls quickly with distance. Then Λ should always be better approximated by a small cluster calculation than Γ. (Despite the fact that Γ has non-local corrections, one can easily show that in the high-dimensional limit, all of the methods discussed here will yield the same self-energy and susceptibilities since the non-local corrections to Γ fall on a set of zero measure points).

In employing the solution to the Parquet equation in a MSMB method we would be able to resolve two major limitations of the current approach: (1) an implementation considering the full frequency and momentum dependent vertex will be devoid of the causality problems associated with the self-energy mixing of the two cluster sizes. (2) The approach constitutes a conserving approximation for the large cluster self-energy. Given these potential gains of a future method, we have to stress the extensive computational demands associated with this approach. While in a Γ based implementation a trivial numerical parallelization of the problem leaves manageable demands, the complex nature of the Parquet approach requires substantial future development.

7. Conclusion

We have introduced a numerically feasible MSMB extension to the DCA. In this method the lattice problem is mapped onto that of two embedded clusters, dividing the problem into three length-scales. Correlations on each of the length-scales are approximated commensurate with the strength of the correlation on the respective scale. The intermediate length-regime, which bridges the explicit treatment of short ranged correlations by means of the QMC to the long ranged dynamical mean-field one, is addressed in a diagrammatic long wavelength approximation based on the two-particle irreducible vertex of the small cluster. The first order approximation to the vertex results in the FLEX but including higher order corrections result in a substantial better multi-scale result when compared to explicit large cluster QMC calculations. This can be attributed to the significance of higher

order diagrams at lower temperatures. We proceeded to show that our MSMB results indicate spin and charge separation, and the obtained velocities compare favorably to a significantly larger finite size QMC calculation. The inclusion of the explicit QMC calculated vertex is currently still limited, but further work in this direction looks promising. However, in any of the introduced implementations, the MSMB approach provides a means to adequately address large cluster problems on all length-scales at significantly lower computational expense.

Acknowledgments

We acknowledge useful conversations with D Hess. This research was supported by grants NSF DMR-0312680, NSF DMR-0113574 and NSF SCI-9619020 through resources provided by the San Diego Supercomputer Center. T Maier and C Slezak acknowledge support from the Center for Nanophase Materials Sciences, Oak Ridge National Laboratory, which is funded by the Division of Scientific User Facilities, US Department of Energy.

Note added in proof. During the completion of this paper we learned of two related studies [25] and [26] where long ranged correlations are addressed in a two-length-scale, non-self-consistent approach.

References

[1] Maier T, Jarrell M, Pruschke T and Hettler M 2005 *Rev. Mod. Phys.* **77** 1027
[2] Jarrell M, Maier T, Huscroft C and Moukouri S 2001 *Phys. Rev.* B **64** 195130
[3] Hague J P, Jarrell M and Schulthess T C 2004 *Phys. Rev.* B **69** 165113
[4] Hubbard J 1963 *Proc. R. Soc.* **276** 276
[5] Müller-Hartmann E 1989 *Z. Phys.* B **74** 507
[6] Metzner W and Vollhardt D 1989 *Phys. Rev. Lett.* **62** 324
[7] Maier T, Jarrell M, Pruschke T and Keller J 2000 *Eur. Phys. J.* B **13** 613
[8] Aryanpour K, Hettler M H and Jarrell M 2003 *Phys. Rev.* B **67** 085101
[9] Mermin N D and Wagner H 1966 *Phys. Rev. Lett.* **17** 133
[10] Vilk Y M and Tremblay A-M S 1997 *J. Physique* I **7** 1309
[11] Baym G 1962 *Phys. Rev.* **127** 1391
[12] Hettler M H, Mukherjee M, Jarrell M and Krishnamurthy H R 2000 *Phys. Rev.* B **61** 012739
[13] Baym G and Kadanoff L P 1961 *Phys. Rev.* **124** 287
[14] Abrikosov A A, Gorkov L P and Dzyaloshinski I E 1975 *Methods of Quantum Field Theory in Statistical Physics* (New York: Dover)
[15] Manske D, Eremin I and Bennemann K H 2001 *Phys. Rev. Lett.* **87** 177005
[16] Deisz J J, Hess D W and Serene J W 1996 *Phys. Rev. Lett.* **76** 1312
[17] Bickers N E, Scalapino D J and White S R 1989 *Phys. Rev. Lett.* **62** 961
[18] Bickers N E and Scalapino D J 1989 *Ann. Phys.* **193** 206
[19] Bickers N E and White S R 1991 *Phys. Rev.* B **43** 8044
[20] Sénéchal D, Perez D and Pioro-Ladrière M 2000 *Phys. Rev. Lett.* **84** 522
[21] Kim C, Matsuura A Y, Shen Z-X, Motoyama N, Eisaki H, Uchida S, Tohyama T and Maekawa S 1996 *Phys. Rev. Lett.* **77** 4054
[22] Preuss R, Muramatsu A, von der Linden W, Dieterich P, Assaad F F and Hanke W 1994 *Phys. Rev. Lett.* **73** 732
[23] Zacher M G, Arrigoni E, Hanke W and Schrieffer J R 1998 *Phys. Rev.* B **57** 6370
[24] de Dominicis C and Martin P 1964 *J. Math. Phys.* **5** 14
[25] Toschi A, Katanin A and Held K 2007 *Phys. Rev.* B **75** 045118
[26] Kusunose H 2006 *J. Phys. Soc. Japan* **75** 054713